Progress In Electromagnetics Research, Vol. 145, 287–298, 2014

Travelling Wave Mechanism and Novel Analysis of the Planar Archimedean Spiral Antenna in Free Space

Teng-Kai Chen[1, 2, *] and Gregory H. Huff[1]

Abstract—While Archimedean spiral antennas were invented a half-century ago, only self-complementary impedance can be evaluated directly from the Babinet's principle. This paper examines the effects of metal width and arm spacing on printed spiral's input impedance. A model is proposed based on examination by decomposition of planar spiral. A closed-form expression for the input impedance of Archimedean spiral antenna is obtained by evaluating the proposed model with conformal mapping techniques. Full-wave numerical simulations, Babinet's principle, and a fabricated antenna demonstrate the accuracy of the proposed model. The expression in this work can be used to find the impedance of a variety of spiral complementary structures analytically. The examination and discussion on the effects of other parameters and features in addition to the spiral itself are also provided through numerical simulation.

1. INTRODUCTION

The Archimedean spiral antenna is well known for its broadband characteristics with circular polarization since its first disclosure in the 1950s by Turner [1]. Curtis proposed the first analytical analysis using wire assumption and semicircle approximation [2]. In 1960, Kaiser proposed the band theory stating that the radiation occurs in the regions where the two filamentary currents on the neighboring wires are in-phase [3]. No rigorous math is described by the band theory, but its easier-understood concept can explain several notable properties of Archimedean spiral antennas. Although there was a dispute that the Archimedean is not a type of frequency independent antenna [4], it shares similar properties with the equiangular spiral and some research report that the Archimedean is a better candidate for broadband application [5, 6].

After those analytical works in the 1960s, the pursuit of a physically descriptive analysis on the Archimedean spiral antenna has received less attention perhaps due to its curvilinear structure and the geometric complexity. A number of numerical methods have been developed and utilized to model these broadband attributes. The method of moments (MoM) with thin-wire assumption is applied in several earlier works to investigate the spiral on an infinite reflector [7], impedance loading along the spiral arms [8], and monofilar spiral backed by a ground plane [9] in free space. The printed wire design can also be analysed by MoM on a semi-infinite dielectric substrate [10], an infinite conductor-backed substrate [11, 12], and an infinite grounded substrate with superstrate [13]. For the printed spiral with non-negligible arm width, the thin-wire assumption is less valid due to the fact that the currents will reside on the edges of metal strip. The analysis of them has been performed using various computational techniques, e.g., the finite-volume time-domain (FVTD) method [14], the finite-difference time-domain (FDTD) method [15–20], the finite element method (FEM) [21], and commercial full-wave solvers [22–25].

Received 19 January 2014, Accepted 21 March 2014, Scheduled 3 April 2014

* Corresponding author: Teng-Kai Chen (tengkaichen@gmail.com).

[1] Department of Electrical and Computer Engineering, Texas A&M University, College Station, TX 77843, USA. [2] Fujitsu Laboratories of America, Inc., Sunnyvale, CA 94085, USA.

These methods have been collectively successful in the analysis of many spiral antennas, but they are not convenient for the design and synthesis. This is especially true with regards to the input impedance, which is very important to feeding the power effectively but fully unpredictable except the self-complementary structure in free space. The pioneered work in [26] applied the concept of the band theory and developed the coplanar strip (CPS) model. Our previous work proposed a model based on a conjectured field distribution of the radiation region similar to what the band theory stated due to the in-phase currents [27]. This work proposes an alternative quasi-static model based on a novel analysis on the planar spiral structure (disregarding the band theory) and provides a rigorous conformal mapping analysis. The primary differentiator from other models is the more accurate treatment of the spiral transmission line as a slotline with finite lateral PMC boundaries. In this paper, the two-arm spiral geometry is reviewed first with its major design parameters and operational assumptions. A model for the quasi-TEM slotline propagating mode is proposed next, and followed by the conformal mapping analysis. Babinet's principle and full-wave electromagnetic simulations verify this analytical closed-form expression. Experimental observations on a fabricated antenna provide additional demonstration on the accuracy of the simulated results and proposed method.

2. ARCHIMEDEAN SPIRAL ANTENNA

Figure 1 shows a non-self-complementary two-arm planar gap-fed Archimedean spiral antenna. The equation of Archimedean spiral curve is given by

$$r = a\theta + r_{\text{in}} \tag{1}$$

where r is the radius of curve, a the growth rate, θ the winding angle, and r_{in} the inner radius of spiral. The outer radius is then defined by $r_{\text{out}} = 2\pi Na + r_{\text{in}}$ with N turns of the spiral. Two edge curves of c_1 and c_2 describe one spiral arm as $c_1 = a\theta + r_{\text{in}}$ and $c_2 = a(\theta + \theta_{\text{off}}) + r_{\text{in}}$, where θ_{off} is the offset angle. The metal width W and the metallization ratio χ of spiral antenna can then be defined as

$$W = |c_1 - c_2| = \theta_{\text{off}} a \tag{2}$$

$$\chi = \frac{W}{W+S} = \frac{\theta_{\text{off}}}{\pi} \tag{3}$$

The design of the trapezoid feed section at the spiral center is shown in the exploded-view in Figure 1 with the taper to a gap length of g and gap width of W_g. The inner radius is designed by

$$r_{\text{in}} = \frac{S}{4\sin\left(\frac{S}{2a}\right)} \tag{4}$$

for parametric study in the following numerical simulation.

Computation of radiation characteristics on spiral antenna has been the subject of several papers, on which the numerical approaches are based mostly, while the band theory provides physical insight into its radiating operation [3]. There is no mathematical rigor attached to this theory, but it surmises

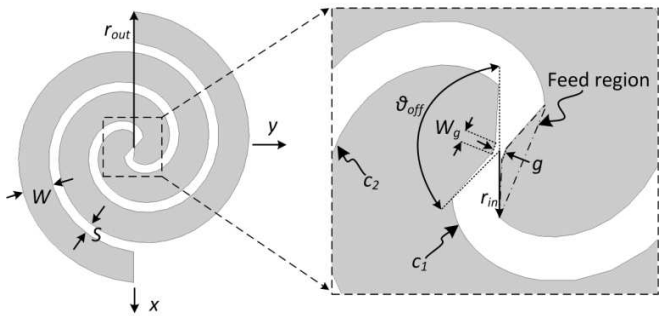

Figure 1. The two-arm planar Archimedean spiral antenna with number of spiral turns of $N = 1.5$ and non-negligible metal width.

that the broadside radiation originates in annular regions where the outward-propagating filamentary currents in neighboring wires are in-phase. This radiating mechanism is geometrically similar to a loop antenna with a circumference that is equal to a guided wavelength λ_g as

$$2\pi r_{\text{rad}} = \lambda_g = \frac{v_p}{f} \tag{5}$$

where r_{rad} is the radius of the loop antenna, v_p is the phase velocity of guided wave, and f is the operating frequency. The lower bound of bandwidth predicted by the band theory can therefore be approximated using r_{out}. For the upper bound of operating frequency, there is historically no prediction of it, but it can be approximated using r_{in} if there is no tapered feed region in the spiral center [28]. In the region between the upper and lower frequency bounds, a band of nearly constant impedance can be seen.

3. PARALLEL SLOTLINE MODEL

For any antenna design, the impedance matching is a key factor to radiate power effectively. Assuming the spiral arms are symmetrically designed with an infinite number of turns and are excited in its fundamental balanced mode, two leaky traveling waves propagate outward from the feed location and a perfect magnetic conductor (PMC) wall can then be placed in the middle perpendicular plane of spiral arm, as shown in Figure 2(a). The treatment is similar to the work in [29]. To investigate its impedance properties, the spiral is then unwrapped into an un-curved two-conductor transmission line, and a short section about the central feed can be examined to analyze the relationship between the excitation at the center and the leaky wave supported by the two spiral arms. Figure 2(b) shows the resulting three-port network obtained from this transformed antenna feed structure, where Port1 is a lumped port representing input terminals of the spiral antenna, and Port2 and Port3 are wave ports terminating the slotline structures with PMC walls on their lateral sides.

Figure 3 shows the simulated S-parameters and port impedance of the three-port network shown in Figure 2(b). The width and slot spacing is fixed at $W + S = 2.5$ mm. The characteristic impedances Z_{02} and Z_{03} are taken directly from full-wave simulation [30] of slotline structure at Port2 and Port3, respectively. The lumped port impedance at Port1 is assigned manually during post-processing as the parallel impedance of Z_{02} and Z_{03}. The low S_{11} is expected in Figure 3 because this assignment facilitates an intuitive impedance matching condition. The S_{21} and S_{31} demonstrate 3 dB power transmission from port1 to port2 and port3, respectively, implying that the power is split equally from the input end to the two slotline modes. It is noted that the slotline with finite PMC boundaries has constant

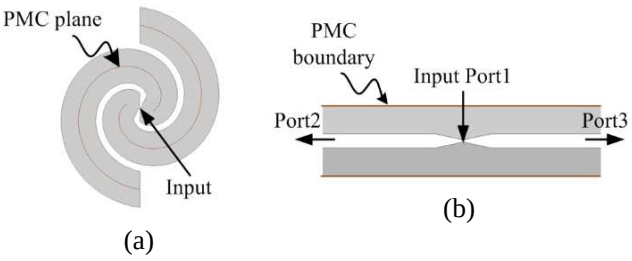

Figure 2. (a) A two-arm planar Archimedean spiral antenna with a perpendicular PMC plane placed along the middle of spiral arms and (b) a three-port network of unwound spiral antenna.

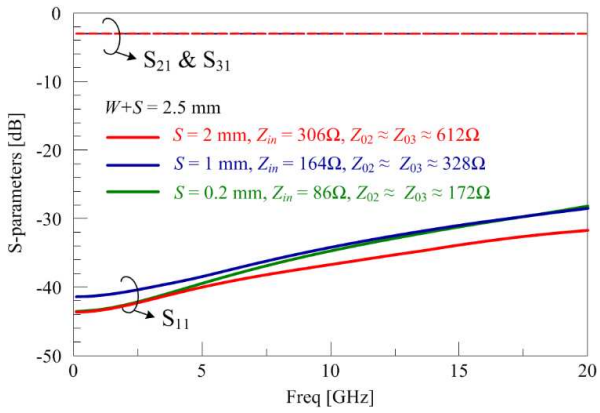

Figure 3. Simulated S-parameters of unwrapped spiral antenna structure.

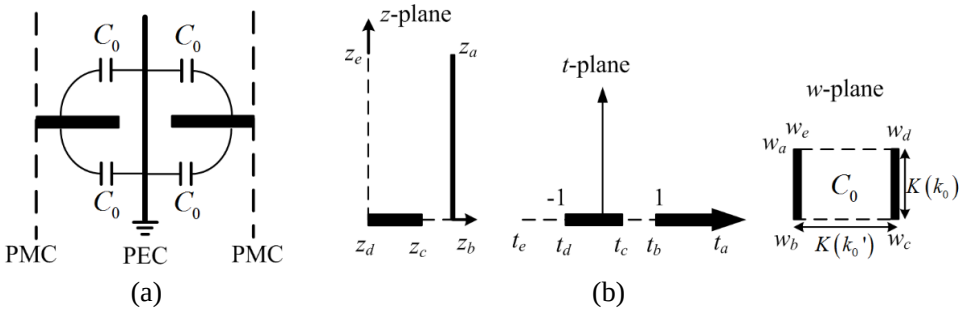

Figure 4. Calculation of capacitance C_0 for slotline mode with lateral PMC in free space; (a) equivalent circuit and (b) conformal mapping steps from z-plane onto t-plane and then onto w-plane.

characteristic impedance from DC up to 50 GHz, while the slotline with infinitely lateral conductor is a highly dispersive transmission line [31].

Based on this examination, the input impedance of spiral antenna is closely related to the parallel characteristic impedance of two outward-propagating slotline modes with lateral PMC boundaries on spiral structures. The quasi-static analysis by conformal mapping [32, 33] is performed here to calculate the characteristic impedance since the potential functions and the capacitances between corresponding conductors are preserved after mapping to a simpler domain for which solutions are easily obtained. Several additional conditions are assumed to retain sufficient accuracy at higher frequencies. First, the quasi-TEM wave propagation will be maintained by ensuring $W + S \ll \lambda_g/2$ for the spiral and slotline. Next, the metal strips have negligible thickness and are PEC. The per-unit-length (*P.U.L.*) capacitance C_0 is the only unknown parameter required to obtain the characteristics. The general mapping processes used in this paper is outlined in the Appendix.

Figure 4(a) shows the cross section of slotline with PMC boundaries, where a PEC wall is placed at the middle plane of slot due to assumed symmetric field distribution. The *P.U.L.* capacitance C_0 can then be evaluated by conformal mapping analysis described in Figure 4(b). The z-plane for this topology has the coordinates $z_b = W/2 + S/2$, $z_c = W/2$ and $z_d = 0$, and the mapping function

$$t = -\cos\left(\frac{2\pi z}{W+S}\right) \tag{6}$$

maps these points onto the t-plane. The parallel-plate structure in the w-plane can be obtained using the transformation in (A3), and C_0 can be obtained by

$$C_0 = \varepsilon_0 \frac{K(k_0)}{K\left(\sqrt{1-k_0^2}\right)} \tag{7}$$

where the modulus of elliptic integral is $k_0 = \sin(\chi\pi/2)$. From the equivalent circuit shown in Figure 4(a), the characteristic impedance Z_0 of slotline are given by

$$Z_0 = \frac{\sqrt{\mu_0\varepsilon_0}}{C_0} \tag{8}$$

where ε_0 and μ_0 are the permittivity and permeability in free space, respectively. The input impedance of spiral antenna can be evaluated by the parallel impedance of Z_0.

4. RESULTS AND DISCUSSIONS

The conformal mapping analysis can provide an accurate prediction across a wide frequency band [34, 35]. Analytical results obtained from quasi-static model are compared in this section to the full-wave simulated results. Moreover, the Babinet's principle demonstrates the accuracy of proposed model.

4.1. Parametric Study of Archimedean Spiral Antenna

The Archimedean spiral antennas with design parameters of $W + S = 5\,\text{mm}$, $N = 5$, and $g = W_g = 0.04 \times W$ are examined to provide a demonstration vehicle for evaluation of proposed model. The radiation boundary is truncated from the radiating source by half wavelength of lower frequency of bandwidth using the band theory of (5) with r_{out}. The maximum size of tetrahedron meshing elements is limited by $W/5$ along the spiral arms for accuracy. Figure 5 shows the simulated input impedance as a function of frequency for $\chi = 0.167$, 0.5, and 0.833. The theoretical frequency span was determined by r_{in} and r_{out} for the upper and lower bounds of 20.042 GHz and 932 MHz, respectively. In practice, the lower frequency has been found to be upwards of three times this theoretical value [23]. Following this, the low frequency limit is $3f_L = 2.795\,\text{GHz}$. The upper limit of 20.042 GHz is somewhat arbitrary since there is no explicit limit to this, but it may be limited in practice by 1/3, which is self-consistent with the lower limit. Thus, a bandwidth approximately from 2.8 GHz to 6.7 GHz is considered here in Figure 5.

Figure 5 shows that the input reactance is close to zero in the radiation region, which is a well-known property of spiral antenna [7, 10, 16]. A clearly frequency-independent behavior of input impedance is observed on the self-complementary structure ($\chi = 0.5$) over the bandwidth. For the structure of $\chi \neq 0.5$, the input impedance is a little offset from the frequency-independent value. This is explained by the difference between frequency-independent antennas and Archimedean spiral antennas [34]. As expected, only the self-complementary structure exhibits frequency-independent behavior. Less frequency-dependence at higher metallization ratios can also be observed due to the more concentrated field distribution in the narrower slot, which makes the *P.U.L.* capacitance of transmission line less dependent on frequency. In general, the analytical conformal mapping results have good agreements with simulated input resistance.

In addition to metallization ratio χ, other spiral parameters may have effects on the input impedance. The lower frequency point of stable impedance is dominated by the outer radius (e.g., $W + S$ and N), but their input resistance remain similar values in the radiation region (supported by numerical simulation but not shown here). Figure 6 shows the simulated input impedance of three Archimedean spirals in different arm termination and feed region. The antennas to be simulated in Figure 6 all have spiral parameters of $W + S = 5\,\text{mm}$ and $N = 5$ with various metallization ratios. In

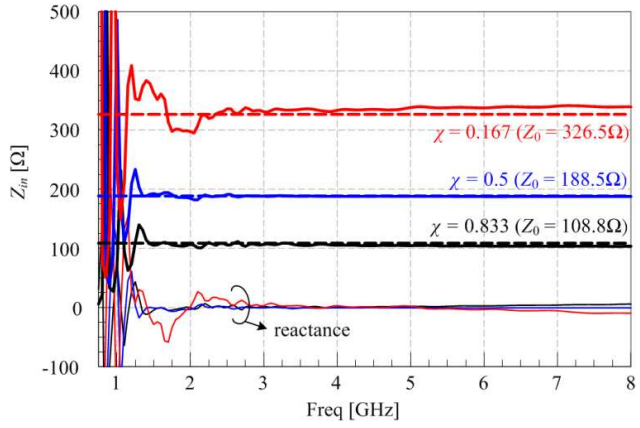

Figure 5. Simulated input impedance (solid line) of two-arm planar Archimedean spiral antenna in free space compared with analytical impedance (dashed line) of parallel slotline model by conformal mapping.

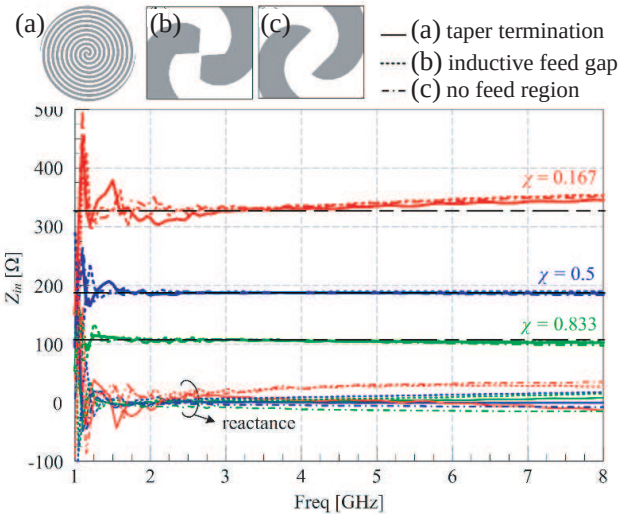

Figure 6. Simulated input impedance of spiral antenna design with (a) taper arm termination, (b) inductive feed region ($g > W_g$), and (c) no feed region.

case (a), the antenna has the feed region of $g = W_g = 0.04 \times W$ and arm termination by a taper to a point to reduce the reflection from the end of the antenna. The input impedance of this case remains similar behavior to Figure 5 in the radiation region because most of the power of propagating mode is radiated without reflecting back from the end. In case (b), the antenna has no arm termination but has the feed region design by $g = 0.1 \times r_{\text{in}}$ and $W_g = 0.04 \times W$, where g is always larger than W_g. This feed gap design has inductive response in the input end rendering the positive input reactance, but the input resistance still remains similar behavior. In case (c), the antenna has no arm termination and no feed region design. The input reactance becomes inductive when the metallization ratio is small due to the small metal arm width, while the input reactance becomes capacitive when the metallization ratio is large. It is noted that the input reactance of self-complementary structure without feed region has capacitive input reactance due to the large input gap as shown in Figure 6(c). Although different feed design may affect the input impedance (mostly on input reactance), the behavior on the input resistance is obviously a function of metallization ratio and can be captured by analytical model very well.

4.2. Parallel Slotline Model and CPS Model

Since a band of nearly constant impedance can be observed between the upper and lower frequency limits, the input resistance at the low frequency operating point is extracted to compare with the proposed quasi-static model. Figure 7 shows a good agreement between the simulated results of gap-fed spiral and those obtained by conformal mapping. The parallel slotline model can predict the input impedance of two-arm gap-fed Archimedean spiral antenna over a suitably wide frequency band, especially for larger metallization ratio.

Results obtained using the CPS model in [26] are also included in Figure 7 for comparison since it provides the first demonstration that conformal mapping techniques can be used to evaluate the impedance of spiral antenna (and any planar non-self-complementary symmetric antenna structure). This model represents a pioneering effort in regards to its approach and insight, but the results in Figure 7 indicate that the CPS model yields different results to those evaluated by parallel slotline model. From physical point of view, the complementary structure of any CPS is interpreted as a CPW with infinite lateral grounds; this is not a self-complementary structure by virtue of CPS and further illustrates why the CPS model cannot obtain the self-complementary impedance of $\eta_0/2 = 188.5\,\Omega$ at $\chi = 0.5$ ($W = S$). Other mathematical differences between the proposed model and the work in [26] reside in its derivation. The CPS model is evaluated by modifying the self-complementary impedance of $\eta_0/2$ using a multiplicative factor. Specifically, this factor uses the ratio of characteristic impedances for a non-complementary CPS ($W_{\text{CPS}} \neq S_{\text{CPS}}$) to the characteristic impedance of self-complementary CPS ($W_{\text{CPS}} = S_{\text{CPS}}$), where W_{CPS} is the metal width, S_{CPS} is the strip spacing, and the impedance of CPS is given by [36]. Strictly speaking, it is not a rigorous derivation directly from a CPS structure.

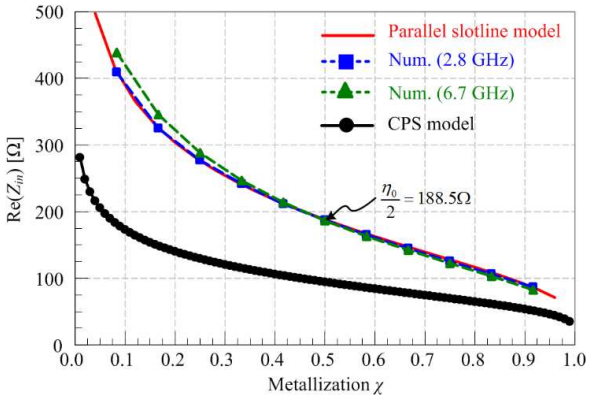

Figure 7. Analytical impedance (parallel slotline model and CPS model in [26]) and simulated input impedance (Num.) of two-arm Archimedean spiral antenna in free space at 2.8 GHz and 6.7 GHz.

4.3. Babinet's Principle

Booker's widely recognized relation of $Z_{\text{metal}}Z_{\text{slot}} = \eta^2/4$ for Babinet's principle in electromagnetic fields [37, 38] can be used to benchmark the proposed parallel slotline model, where Z_{metal} and Z_{slot} are the input impedances of metal and slot radiating modes, respectively, and η is the intrinsic impedance. This principle is of fundamentally importance and can be applied to find the impedance for a wide variety of complementary structures. However, it cannot provide a priori information for non-self-complementary spiral antennas since Z_{metal} and Z_{slot} are typically unknown.

For an Archimedean spiral antenna with a metallization ratio of χ, its complementary structure has a metallization ratio of $(1-\chi)$ and the input impedance Z_{in}^c is given by

$$Z_{\text{in}}^c = \frac{1}{2}\sqrt{\frac{\mu_0}{\varepsilon_0}}\frac{K\left[\sin\left(\pi\frac{\chi}{2}\right)\right]}{K\left[\cos\left(\pi\frac{\chi}{2}\right)\right]} \tag{9}$$

Multiplying the impedance of $Z_{\text{in}} = Z_0/2$ and its complementary impedance of Z_{in}^c, the result is given by

$$Z_{\text{in}} \times Z_{\text{in}}^c = \frac{\eta_0^2}{4} \tag{10}$$

where $(\mu_0/\varepsilon_0)^{1/2} = \eta_0$. This demonstrates that the expression fulfills the relationship of complementary structures and accurately predicts the input impedance of Archimedean spiral antenna. Since (8) is a function of only metallization ratio, it is reasonable to deduce that the impedance derived by conformal mapping can be generalized for any planar complementary FI structure.

5. MEASUREMENT

A two-arm gap-fed Archimedean spiral antenna was fabricated and measured for further verification of conformal mapping result. The prototype antenna has metallization ratio of $\chi = 0.8333$ with $W+S = 30\,\text{mm}$. The input region design has $g = 0.5\,\text{mm}$ and $W_g = 0.25\,\text{mm}$. The outer radius of spiral is 99.6 mm and consists of turns $N = 1.5$. These parameters were determined by the limitations of the mechanical milling area and the capability of carrying cable on spiral arms. The antenna was milled from solder-tacked copper tape atop a $228.6\,\text{mm} \times 228.6\,\text{mm}$ square Rohacell 51 IG (polymethacrylimide foam) substrate [39] with dielectric constant $\varepsilon_r = 1.05$, loss tangent $\tan\delta = 0.003$, and a thickness of 3.99 mm. The foam provided physical support for the antenna while remaining closely matched in material properties to free space. The backside of fabricated antenna has no conductor plane. The infinite balun design in [40] is adopted as a feed, which requires a wide metal arm to carry the feeding cable along the middle of spiral arm. The dummy cable on the other arm is necessary to remain the symmetry of spiral structure. The length of coaxial cable is 914.4 mm for de-embedding the measured point to the input terminal of spiral antenna. The impedance measurements were obtained by Agilent E8361C VNA using port extension to move the reference plane electrically to spiral center.

Figure 8 shows measured and simulated input impedances from 500 MHz to 8 GHz. The average measured and simulated real-valued impedances from 1 GHz to 8 GHz are $106.02\,\Omega$ and $111.69\,\Omega$, respectively, while the conformal mapping result is $108.7527\,\Omega$. As expected, the presence of additional metal surfaces from cables and solder increases the capacitive loading on transmission line and hence decreases the characteristic impedance of slotline mode. The experimental data are however in reasonable good agreement with the simulated results. It is noted that the measured input reactance of this spiral is $-10^{-4}\,\Omega$, while the simulated input reactance is around $11\,\Omega$. The positive input reactance is due to the inductive feed region design and the capacitive loading of soldered cable across the input terminal compensates this inductive reactance.

Although the radiation patterns of spiral antenna are well studied in literatures, not the focus in this work, the measured radiation pattern is included here for readers' interest. The gain measurements were obtained through anechoic chamber. Figure 9 shows the measured and simulated radiation pattern (E_θ and E_φ) in xz- and yz-plane at different frequencies within the radiation bandwidth of the spiral antenna. Due to the impedance mismatch between the input impedance of spiral antenna and characteristic impedance of coaxial cable, the realized gain of simulated result is recorded in this

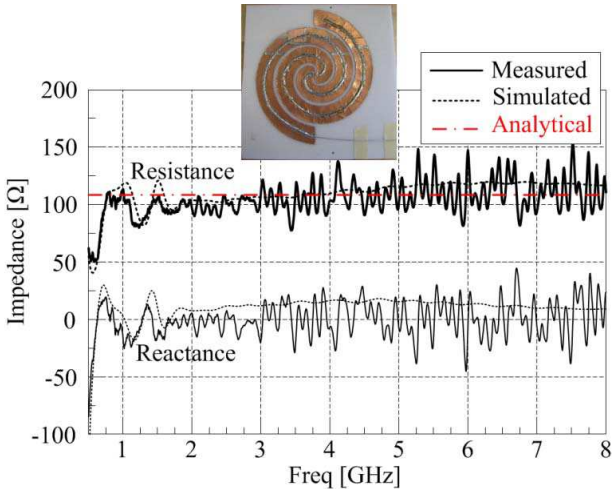

Figure 8. Measured input impedance (solid line) after de-embedded calibration of cable, simulated input impedance (dashed line) without the infinite balun, and conformal mapping result (red dash-dot line) of the fabricated spiral antenna.

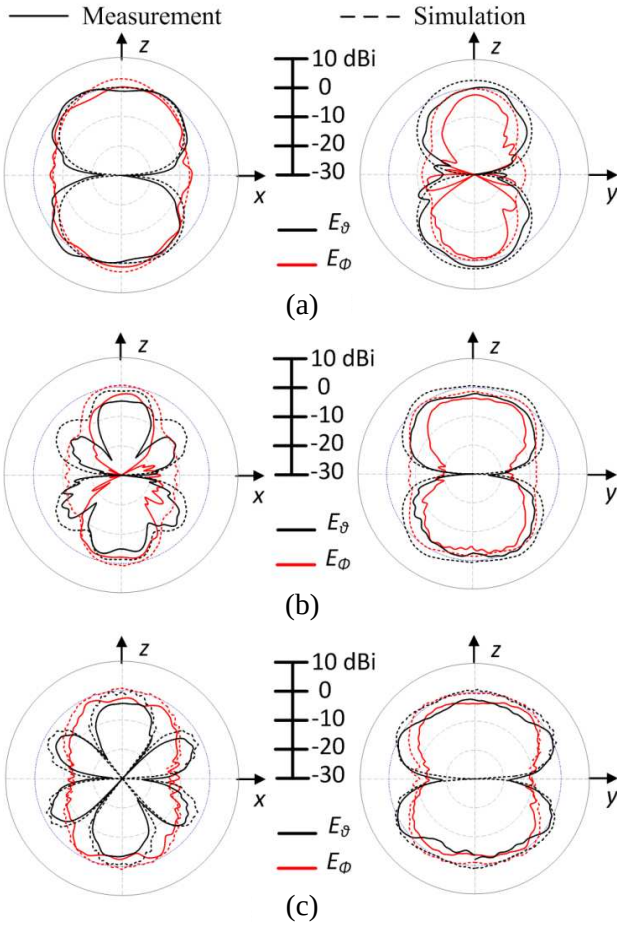

Figure 9. Radiation patterns of measured gain (solid line) and simulated realized gain (dashed line) in xz- and yz-plane at (a) 3 GHz, (b) 6 GHz, and (c) 8 GHz.

plot. The discrepancy between the peak measured and simulated radiation patterns is mainly due to the cable loss, i.e., the simulation performed by an ideal input without the long feeding cable along the spiral arms to the input end. Other reasons may be due to the imperfect fabrication by our lab equipment and additional mismatch interaction between the coaxial transitions to the DUT. Taking the cable loss into consideration (e.g., 2.30 dB/m at 3 GHz and 4.27 dB/m at 10 GHz), the simulated radiation pattern has a very good agreement with the measured one. The axial ratio is below 5 dB across the radiation bandwidth (not shown here), while it can be improved by increasing the spiral turns. It is worthy to note that this antenna design has not been optimized in any way or chosen for any particular performance attribute.

6. CONCLUSION

A rigorous analysis and a closed-form expression for the input impedance of Archimedean spiral antenna have been obtained using the parallel slotline model, which gives physical insight when the spiral arm width is non-negligible (cannot be considered as thin wires). Other spiral parameters such as the number of turns and the spiral growth rate have little effect on the input impedance operating at its radiation region, while the feed design may affect the impedance since it is placed near the input terminal. The accuracy of derived expressions has been verified by three ways: comparison with the numerical results by full-wave solver, substitution into the Babinet's principle, and measurement of fabricated antenna. The proposed analysis provides an accurate prediction for the input impedance of Archimedean spiral antenna in free space.

It is worthy to note that expression (8) is only a function of metallization ratio, which indicates that it may be applied to other frequency-independent antennas based on traveling wave mechanism. The closed-form expression in this work is important because it is not found since Archimedean spiral antennas were invented a half-century ago. Only self-complementary impedance can be evaluated directly from the Babinet's principle in most of antenna textbook and spiral antenna literatures. It can be applied to find the impedance of a variety of spiral complementary structures analytically, while the Booker's relation can only be used to find the self-complementary impedance. It can also be applied to design spiral antenna's impedance to match with system impedance since it is hard to design a wideband balun as wide as the frequency response of spiral antenna [41, 42]. It is especially useful for any spiral antenna design starting from designing input impedance as works in [43].

APPENDIX A.

The Schwartz-Christoffel transformation [44] provides a useful tool to calculate capacitance and is given by

$$\frac{df\,(t)}{dt} = \prod_{\rho=1}^{n} (t - t_\rho)^{-(1-\alpha_\rho)} \tag{A1}$$

where $w = f(t)$ is the mapping function. It maps the upper-half of complex t-plane onto the interior of a polygon in w-plane and the real axis onto the boundary with the interior angle of $\pi\alpha_\rho$ at the vertex ρ of polygon. For a closed convex polygon, the restriction on α_ρ is given by

$$\sum_{\rho=1}^{n} (1 - \alpha_\rho) = 2 \tag{A2}$$

For more than four vertices ($n > 4$), this transformation can only be evaluated by numerical integration. Fortunately, the transformation for calculation of parallel-plate capacitance can be expressed by a linear combination of elliptic integrals.

Figure A1 shows the general transformation when mapping the upper half-plane onto the interior of the rectangle with $\alpha_k = 1/2$ and $n = 3$ by

$$w = A + B \int^{t} \prod_{\rho=1}^{3} \left(t' - t_\rho\right)^{-\frac{1}{2}} dt' \tag{A3}$$

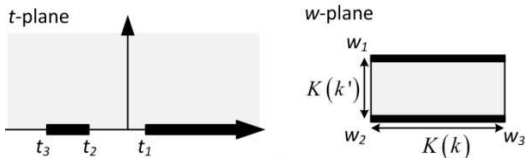

Figure A1. Schwartz-Christoffel transformation of $n = 3$.

where constant A describes a translation and constant B describes the rotation and magnification. For a generic value of t, the integral is said to be incompletely expressed by the elliptic integral of first kind as

$$F(\varphi, k) = \int_0^{\sin\varphi} \frac{dx}{\sqrt{(1-x^2)(1-k^2x^2)}} \tag{A4}$$

where φ and k are called amplitude and modulus of elliptic integrals, respectively.

When $\varphi = \pi/2$, the integration in (A4) can be expressed as $K(k)$; this expression is called the complete elliptic integral of first kind. The integral in (A3) can be found in a table of integrals (e.g., [45]), and the boundary of the rectangle in the w-plane are given by

$$\int_{t_3}^{t_2} \frac{dt'}{\sqrt{(t'-t_1)(t'-t_2)(t'-t_3)}} = -g_3 K(k) \tag{A5}$$

$$\int_{t_2}^{t_1} \frac{dt'}{\sqrt{(t'-t_1)(t'-t_2)(t'-t_3)}} = j g_3 K\left(k'\right) \tag{A6}$$

where the geometric parameters are expressed in

$$g_3 = \frac{2}{\sqrt{(t_1-t_3)}} \tag{A7}$$

$$k = \sqrt{\frac{(t_2-t_3)}{(t_1-t_3)}} \tag{A8}$$

and $k' = (1-k^2)^{1/2}$ is the complementary modulus of elliptic integral. It is noteworthy that the parameter g_3 is not shown in Figure A1 since it represents the magnification of mapping and will be canceled in the calculation of capacitance.

REFERENCES

1. Turner, E. M., "Spiral slot antenna," United States Patent US2863145 A, 1958.
2. Curtis, W., "Spiral antennas," *IRE Trans. Antennas Propag.*, Vol. 8, No. 3, 298–306, 1960.
3. Kaiser, J., "The Archimedean two-wire spiral antenna," *IRE Trans. Antennas Propag.*, Vol. 8, No. 3, 312–323, 1960.
4. Dyson, J. D., R. Bawer, P. E. Mayes, and J. I. Wolfe, "A note on the difference between equiangular and Archimedes spiral antennas (correspondence)," *IRE Trans. Microw. Theory Tech.*, Vol. 9, No. 2, 203–205, 1961.
5. Lacko, P., "Archimedean-spiral and log-spiral antenna comparison," *Proc. SPIE*, Vol. 4742, No. 1, 230, 2002.
6. Paolino, D., "Reduced-size spiral antenna design using dielectric overlay loading for use in ground penetrating radar and design of alternative antennas using Vivaldi radiators," *Proc. SPIE*, Vol. 4742, No. 1, 218, 2002.
7. Nakano, H., K. Nogami, S. Arai, H. Mimaki, and J. Yamauchi, "A spiral antenna backed by a conducting plane reflector," *IEEE Trans. Antennas Propag.*, Vol. 34, No. 6, 791–796, 1986.

8. Champagne, II, N. J., J. T. Williams, R. M. Sharpe, S. U. Hwu, and D. R. Wilton, "Numerical modeling of impedance loaded multi-arm Archimedean spiral antennas," *IEEE Trans. Antennas Propag.*, Vol. 40, No. 1, 102–108, 1992.
9. Nakano, H., Y. Shinma, and J. Yamauchi, "A monofilar spiral antenna and its array above a ground plane-formation of a circularly polarized tilted fan beam," *IEEE Trans. Antennas Propag.*, Vol. 45, No. 10, 1506–1511, 1997.
10. Nakano, H., K. Hirose, I. Ohshima, and J. Yamauchi, "An integral equation and its application to spiral antennas on semi-infinite dielectric materials," *IEEE Trans. Antennas Propag.*, Vol. 46, No. 2, 267–274, 1998.
11. Li, R.-L. and H. Nakano, "Numerical analysis of arbitrarily shaped probe-excited single-arm printed wire antennas," *IEEE Trans. Antennas Propag.*, Vol. 46, No. 9, 1307–1317, 1998.
12. Khamas, S. K. and G. G. Cook, "Moment-method analysis of printed wire spirals using curved piecewise sinusoidal subdomain basis and testing functions," *IEEE Trans. Antennas Propag.*, Vol. 45, No. 6, 1016–1022, 1997.
13. Khamas, S. K., P. L. Starke, and G. G. Cook, "Design of a printed spiral antenna with a dielectric superstrate using an efficient curved segment moment method with optimisation using marginal distributions," *IEE Proc. Microw. Antennas Propag.*, Vol. 151, No. 4, 315–320, 2004.
14. Fumeaux, C., D. Baumann, and R. Vahldieck, "Finite-volume time-domain analysis of a cavity-backed Archimedean spiral antenna," *IEEE Trans. Antennas Propag.*, Vol. 54, No. 3, 844–851, 2006.
15. Penney, C. W. and R. J. Luebbers, "Input impedance, radiation pattern, and radar cross section of spiral antennas using FDTD," *IEEE Trans. Antennas Propag.*, Vol. 42, No. 9, 1328–1332, 1994.
16. Nakano, H., H. Yasui, and J. Yamauchi, "Numerical analysis of two-arm spiral antennas printed on a finite-size dielectric substrate," *IEEE Trans. Antennas Propag.*, Vol. 50, No. 3, 362–370, 2002.
17. Nakano, H., M. Ikeda, K. Hitosugi, and J. Yamauchi, "A spiral antenna sandwiched by dielectric layers," *IEEE Trans. Antennas Propag.*, Vol. 52, No. 6, 1417–1423, 2004.
18. Nakano, H., R. Satake, and J. Yamauchi, "Extremely low-profile, single-arm, wideband spiral antenna radiating a circularly polarized wave," *IEEE Trans. Antennas Propag.*, Vol. 58, No. 5, 1511–1520, 2010.
19. Nakano, H., T. Igarashi, H. Oyanagi, Y. Iitsuka, and J. Yamauchi, "Unbalanced-mode spiral antenna backed by an extremely shallow cavity," *IEEE Trans. Antennas Propag.*, Vol. 57, No. 6, 1625–1633, 2009.
20. Afsar, M. N., W. Yong, and R. Cheung, "Analysis and measurement of a broadband spiral antenna," *IEEE Antennas Propag. Mag.*, Vol. 46, No. 1, 59–64, 2004.
21. Li, R. and G. Ni, "Numerical analysis of 4-arm Archimedian printed spiral antenna," *IEEE Trans. Magn.*, Vol. 33, No. 2, 1512–1515, 1997.
22. Zhou, D., S. Gao, R. A. Abd-Alhameed, C. Zhang, M. S. Alkhambashi, and J. D. Xu, "Design and optimisation of compact hybrid quadrifilar helical-spiral antenna in GPS applications using genetic algorithm," *2012 6th European Conference on Antennas and Propagation (EUCAP)*, 1–4, 2012.
23. Gschwendtner, E. and W. Wiesbeck, "Ultra-broadband car antennas for communications and navigation applications," *IEEE Trans. Antennas Propag.*, Vol. 51, No. 8, 2020–2027, 2003.
24. Bell, J. M. and M. F. Iskander, "A low-profile Archimedean spiral antenna using an EBG ground plane," *IEEE Antennas Wireless Propag. Lett.*, Vol. 3, No. 1, 223–226, 2004.
25. Muller, D. J. and K. Sarabandi, "Design and analysis of a 3-arm spiral antenna," *IEEE Trans. Antennas Propag.*, Vol. 55, No. 2, 258–266, 2007.
26. Huffman, J. A. and T. Cencich, "Modal impedances of planar, non-complementary, N-fold symmetric antenna structures," *IEEE Antennas Propag. Mag.*, Vol. 47, No. 1, 110–116, 2005.
27. Chen, T.-K. and G. H. Huff, "Modal resistance of spiral antenna," *J. Electromagn. Anal. Appl.*, Vol. 5, No. 5, 223–228, 2013.
28. Nakano, H., S. Sasaki, H. Oyanagi, and J. Yamauchi, "Cavity-backed Archimedean spiral antenna with strip absorber," *IET Microw. Antennas Propag.*, Vol. 2, No. 7, 725–730, 2008.

29. Chen, T.-K. and G. H. Huff, "Design and analysis of a stripline Archimedean snail antenna," *PIERS Proceedings*, 775–779, Taipei, Mar. 25–28, 2013.
30. HFSS, V12.0, Ansoft Corporation, Pittsburgh, PA, 2010.
31. Gupta, K. C., R. Garg, I. Bahl, and P. Bhartia, *Microstrip Lines and Slotlines*, 2nd Edition, Artech House, Norwood, Massachusetts, 1996.
32. Collin, R. E., *Foundations for Microwave Engineering*, 2nd Edition, Wiley-IEEE Press, New York, 2000.
33. Chen, T.-K. and G. H. Huff, "Analytical investigation of periodic coplanar waveguides," *Progress In Electromagnetics Research M*, Vol. 30, 167–181, 2013.
34. Bedair, S. S. and I. Wolff, "Fast, accurate and simple approximate analytic formulas for calculating the parameters of supported coplanar waveguides for (M)MIC's," *IEEE Trans. Microw. Theory Tech.*, Vol. 40, No. 1, 41–48, 1992.
35. Ghione, G. and C. U. Naldi, "Coplanar waveguides for MMIC applications: Effect of upper shielding, conductor backing, finite-extent ground planes, and line-to-line coupling," *IEEE Trans. Microw. Theory Tech.*, Vol. 35, No. 3, 260–267, 1987.
36. Chang, K., I. Bahl, and V. Nair, *RF and Microwave Circuit and Component Design for Wireless Systems,* John Wiley & Sons, New York, 2002.
37. Booker, H. G., "Slot aerials and their relation to complementary wire aerials (Babinet's principle)," *J. Inst. Elect. Eng. — Part IIIA: Radiolocation*, Vol. 93, No. 4, 620–626, 1946.
38. Deschamps, G., "Impedance properties of complementary multiterminal planar structures," *IRE Trans. Antennas Propag.*, Vol. 7, No. 5, 371–378, 1959.
39. ROHACELL® Structural Foam, Evonik Industries AG, Essen, Germany, 2013.
40. Dyson, J., "The equiangular spiral antenna," *IRE Trans. Antennas Propag.*, Vol. 7, No. 2, 181–187, 1959.
41. Tu, W.-H., M.-Y. Li, and K. Chang, "Broadband microstrip-coplanar stripline-fed circularly polarized spiral antenna," *Proc. IEEE AP-S Int. Symp.*, 3669–3672. 2006.
42. Thaysen, J., K. B. Jakobsen, and J. Appel-Hansen, "A wideband balun — How does it work?," *Appl. Microw. Wireless*, Vol. 12, No. 10, 40–50, 2000.
43. Chen, T.-K. and G. H. Huff, "Stripline-fed Archimedean spiral antenna," *IEEE Antennas Wireless Propag. Lett.*, Vol. 10, 346–349, 2011.
44. Driscoll, T. A. and L. N. Trefethen, *Schwarz-Christoffel Mapping*, Cambridge University Press, Cambridge, UK, 2002.
45. Gradshteifin, I. S. and I. M. Ryzhik, *Table of Integrals, Series and Products*, 7th Edition, Academic Press, Oxford, UK, 2007.